J. Fluid Mech. (1999), *vol.* 382, *pp.* 245–262. Printed in the United Kingdom

© 1999 Cambridge University Press

A note on tuning in Roseau's alternative edge waves

By ULF TORSTEN EHRENMARK

Department of CISM, London Guildhall University, London EC3N 1JY, UK

(Received 6 April 1998)

Ursell's edge waves are derived systematically using a new method. Computed profiles are then compared with the lesser known shoreline singular waves first constructed by Roseau (1958). A recent method of writing the continuous spectrum solutions on a plane beach is thereby extended to the discrete spectrum to enable the reconstruction of both types of edge waves so that, in particular, the unbounded wave profiles are more easily computed. The existence of stagnation points on the bed for standing edge waves is considered and demonstrated for the first few modes. A ramification of this is the existence of (two-dimensional-cross-shore) dividing 'streamlines' from the bed to the surface also, the number of which appears to equate to the modal number of the edge wave. These dividing streamlines, along with other streamlines, are computed for the first few modes of both the Ursell and the (alternative) singular waves constructed by Roseau.

It follows that these waves can also exist in the presence of solid cylinders bounded by fixed streamlines and, in particular therefore, that the hitherto unbounded Roseau waves can exist in a bounded state since a region including the origin can be removed from the flow by exploiting a dividing streamline. It is confirmed that the wavenumbers of the Roseau waves interlace those of the Ursell waves. An examination of available evidence leaves open to further research the question of whether the alternative Roseau waves have been 'inadvertently' observed either in the laboratory or, by means of contamination of data, in the field. Further laboratory simulations using longshore solid cylinders as 'wave guides' are proposed.

1. Introduction

The theory of bounded edge waves on a plane beach is well established. In his seminal work, Ursell (1952) writes the complete set of bounded edge wave solutions possible on an infinite plane beach within the framework of a linear inviscid theory and presents experimental laboratory evidence of the existence both of modes at cut-off (the supremum in the continuous spectrum of the wavenumber) and the edge wave modes which increase in number as the beach angle α is decreased. Further evidence of existence has been given by, amongst others, Guza & Bowen (1976) from laboratory experiments and by Oltman-Shay & Guza (1987) from field tests. The latter work describes evidence of several modes on two different beaches of typical slopes 0.06 and 0.02. The inviscid theory of Ursell, having established the relationship $\omega^2 = gk \sin(2n+1)\alpha$ between angular frequency ω and wavenumber k, shows that the number n of modes possible is always the integer part of $\frac{1}{2} + (\pi/4\alpha)$. Whilst most of the results presented by Oltman-Shay & Guza point to significant peaks at modes 0 and 1, there are substantial observations of energetics at higher modes particularly

https://doi.org/10.1017/S0022112098003899 Published online by Cambridge University Press

for the higher frequency oscillations. Moreover, in one experiment in particular (figure 13 therein), there is a fairly uniform spread of power across the wavelengths between modes 0 and 2 for frequencies in the range 0.033–0.05 Hz. This particular observation is not discussed.

Ursell refers to the work of Peters (1952) for a complete discussion of the continuous spectrum solutions although the first writer to develop such three-dimensional solutions was Roseau (1951). The non-referencing by both Ursell and Peters of this earlier work is easier to understand than is the failure of Roseau (1958) to acknowledge the work of Ursell, since the 1958 work essentially rederives the edge waves already discovered. Whitham (1979) later remarked however that Ursell had indeed written the solutions but had not divulged to his readers the method of discovery. However, in his conclusions, Ursell states his obligation to Dr C. Eckart for discussions leading to the discovery of the critical angles where new modes appear.

The presentation by Roseau (1958) of the bounded edge waves is somewhat different to Ursell's and the intrinsic results are hard to extrapolate from the rigorous and extensive work in proving the various solutions. However, the reader wishing to relate directly to Ursell's edge waves can find a full expression in Roseau (1958, p. 458), the first mode of which is given as a special case (Stokes wave) on p. 463. Moreover, as Roseau saw his work (1958) as a natural extension to $k \geqslant \omega^2/g$ having earlier studied the continuous spectrum $k < \omega^2/g$ (1951), it was natural for him to include the weakly unbounded solutions which, in the latter case certainly, were required for the satisfactory construction of incoming progressing waves. In fact, Roseau also discussed strongly unbounded solutions but these will not be required for the purposes of the present investigation although some of the salient points of the conclusions herein might, in due course, be shown also to apply to these.

Other significant contributions to the theory of edge waves include Whitham (1976), Minzoni (1976), Minzoni & Whitham (1977), Evans (1988, 1989), Miles (1990*a*) and Blondeaux & Vittori (1995). Of these, both Whitham and Minzoni demonstrated non-uniformity at large distances of the shallow-water-approximation edge waves whilst Minzoni & Whitham later considered the excitation of subharmonic edge waves by weakly nonlinear interaction with a classical bounded standing wave normally incident to the shore line (they stated that their methods might also be extended to the case of oblique incidence) and simultaneously showed that the non-uniformity was mild and could be removed by coordinate straining. More recently Blondeaux & Vittori (1995) extended the weak nonlinear theory to discuss the excitation (by the same two-dimensional classical bounded standing wave $a\phi_{00}$) of synchronous edge waves, also through interaction with subharmonic edge waves. Of the various two-parameter interactions considered by them, the interaction of $a\phi_{00}$ with itself was not discussed but this has since been the subject of a separate investigation by Body & Ehrenmark (1999). Meanwhile, Evans, within the framework of a linear theory, had discussed alternative generation mechanisms by considering bottom protrusions and surface pressure disturbances. A recent survey of edge wave work is given by Evans & Kuznetsov (1997).

Most authors (e.g. Whitham 1979; Minzoni & Whitham 1977; Blondeaux & Vittori 1995) reject the inclusion of the weakly singular standing wave, both for the continuous spectrum solutions and for edge wave discussions. This neglect is more harmful in the former case, since it is impossible to construct progressing waves without it. One may ask whether, in the interests of securing a physically meaningful result very near the shoreline where the linear inviscid theory has long

https://doi.org/10.1017/S0022112098003899 Published online by Cambridge University Press

since lost its validity, it is worth sacrificing the fundamentally observed nature of non-breaking incident waves on a beach, namely their dominantly progressive state. Miles (1990*b*) enriches this debate with a shallow-water-expansion matching model where an incoming arbitrary wave is gradually converted to be dominated by standing wave behaviour near the shore line thus enabling the field there to be described through a bounded function by including both viscous and capillary effects. There are numerical limitations to Miles' results (see Ehrenmark 1996) but no doubt a more general viscous model (were this to be possible) would secure the comprehensive conclusion that Miles' interpretation is essentially correct and the far-field flow must, in general, include a term which is at least logarithmically singular at the shore line. This is the view adopted in the present work which is mainly, although not exclusively, focused on computations of the 'weakly singular edge waves'.

The outline of the present work is that, following the brief formulation of general solutions in the next section, the regular (Ursell) and singular (Roseau) edge waves are reconstructed respectively in §§ 3 and 4 by a method developed recently for the continuous spectrum solutions (Ehrenmark 1998, referred to as EH1 hereafter). Following this, Roseau modes are now readily computed and, in particular, a near-field expansion is given which may be used on any desk-top computer. The occurrence of stagnation points on the bed are discussed in connection with dividing streamlines in § 5 and computation procedures are outlined. One of the chief results, that Roseau edge wave modes can exist in a bounded state in the presence of solid longshore orientated cylindrical 'guides', is discussed numerically for a number of cases and in § 6 the possible implications of this are discussed in terms of exisiting data. The conclusion is that further laboratory or field work is required to examine the chances of the modes being realized experimentally. Some concluding remarks are made in § 7.

2. Formulation of solutions

An ansatz for developing three-dimensional solutions to the classical beach problem, in terms of the inverse Kontorovich–Lebedev transform (K–L), is described in full detail in EH1. The main advantages of this method are two-fold. On the one hand there is readily available a nearshore asymptotic expansion which can be used to great accuracy over many wavelengths from the shore line whilst, at the same time, the full expansion permits now established methods for the numerical inversion of K–L to be used to enable reasonably easy computation of the solutions at all distances and all depths regardless of incidence angle. The only restriction with the ansatz is that, for waves below cut-off mode (i.e. continuous spectrum), beach angles are restricted to rational multiples of π of the form $(2p+1)/2q$; $p, q \in \boldsymbol{N}$. For more general beach angles, the solution first given by Roseau (1952) or Peters (1952) would need to be adopted.

The geometry is defined with the z-axis being taken along the shoreline, x directed out to sea and y taken vertically upwards with $y = 0$ as the still water level (SWL). Monochromatic waves of angular frequency ω (here regarded as fixed)† and potential

† Many works take wavenumber fixed and develop instead a spectrum in ω whence its discreet part will then be below the continuous part . We follow Roseau (1958) who thought of the waves as 'short waves' at fixed frequency rather than low-frequency waves at fixed wavelength (infragravity waves).

https://doi.org/10.1017/S0022112098003899 Published online by Cambridge University Press

'amplitude' a are then described in deep water by the potential function

$$\Phi_\infty = a\,\mathrm{Re}\,\{\phi_\infty \exp(\mathrm{i}\omega t)\},$$

where

$$\phi_\infty = \exp\{\mathrm{i}(nx + kz)\}\mathrm{e}^{my}$$

and where the angle of departure γ from incidence along a line of greatest slope is given by $\cos\gamma = n/m$, $\sin\gamma = k/m$. From the Laplace equation it follows that

$$n^2 + k^2 = m^2. \tag{2.1}$$

Non-dimensional variables are taken based on ω and the wavelength at infinity $2\pi/m$, $m = \omega^2/g$. The new radial polar coordinate is $R = r\omega^2/g$, where $x = r\cos\theta$, $y = r\sin\theta$ and the polar line $\theta = 0$ is the SWL whilst the impermeable bed is given by $\theta = -\alpha$. The dimensional variables are non-dimensionalized using off-shore wavenumber and phase speed. Writing $\Phi = a\,\mathrm{Re}\,\{\phi(R,\theta)\exp(\mathrm{i}t)\,\mathrm{e}^{\mathrm{i}kz}\}$, where $g^2\Phi/\omega^3$ is the dimensioned potential, the system for the dimensionless potential function ϕ may be taken in the form

$$(\Delta - \kappa^2)\phi = 0; \quad \{0 < R < \infty, -\alpha < \theta < 0\}, \tag{2.2}$$

$$\phi_\theta(R, -\alpha) = 0; \quad \{0 < R < \infty\}, \tag{2.3}$$

$$\phi_\theta(R, 0) = R\phi(R, 0); \quad \{0 < R < \infty\}, \tag{2.4}$$

$$\lim_{R\to\infty}\{\phi - \phi_\infty\} = 0; \quad \{-\alpha < \theta < 0\}, \tag{2.5}$$

$$\lim_{R\to 0}\{\phi/\ln R\} = -\lambda; \quad \{\lambda\ \text{constant}\}. \tag{2.6}$$

In the above $\kappa = k/m$, the suffix θ denotes a partial derivative and it is understood that the two-dimensional Laplacian Δ is also dimensionless. Note that for edge waves (k above cut-off, $\kappa > 1$), the value of γ in the above would be complex.

A formal solution of (2.2) which satisfies (2.3) is

$$\phi(R,\theta) = \lambda K_0(\kappa R) + \int_0^\infty A(s)\cosh s(\theta + \alpha)\,K_{is}(\kappa R)\,\mathrm{d}s, \tag{2.7}$$

where K_ν is Macdonald's function of order ν (Watson 1944) and λ is a suitable constant. It has been shown in EH1 that $\lambda = -\frac{1}{2}\mathrm{i}\pi\kappa\sin\alpha\,\chi_0$ where χ_0 is the residue of $A(s)$ at the simple pole $s = -\mathrm{i}$ (if A is regular there, $\lambda = 0$). The development of $A(s)$, as the solution of a second-order functional equation, for the case $\kappa < 1$, was given fully in EH1 and will not be repeated here. It is in fact possible to determine discrete spectrum ($\kappa \geqslant 1$) solutions also from the forms given for $\kappa < 1$ by systematically eliminating terms with growing exponentials by restricting slope angles. This procedure is a little *ad hoc* however, and it seems prudent, particularly in view of Whitham's (1979) remark that a systematic derivation is not found in the literature, to return to the general solution. Here $A(s)$ is constructed by the use of a discrete Fourier transform (see EH1 for full details)

$$A(s) = \frac{\Xi(s)}{\sinh s\alpha}\sum_{j=-J}^{J} a_j\,\mathrm{e}^{js\alpha}, \tag{2.8}$$

where Ξ is i-periodic and $J \in \boldsymbol{Z}$. In the above, the a_j satisfy

$$a_{j-1}\left\{\mathrm{e}^{\mathrm{i}\alpha(j-1)} - 2\mathrm{i}\kappa^{-1} - \mathrm{e}^{-\mathrm{i}\alpha(j-1)}\right\} = a_{j+1}\left\{\mathrm{e}^{\mathrm{i}\alpha(j+1)} + 2\mathrm{i}\kappa^{-1} - \mathrm{e}^{-\mathrm{i}\alpha(j+1)}\right\} \tag{2.9}$$

https://doi.org/10.1017/S0022112098003899 Published online by Cambridge University Press

and the solvability condition for the basic functional equation is

$$\kappa^{-1} = \sin\,\alpha J. \tag{2.10}$$

In view of the structure of (2.9) it is clearly desirable to distinguish between even and odd J.

3. Ursell's edge waves

The case $J = 2N + 1,\ N \in \boldsymbol{Z}$ is considered first. It is easy to show from the recurrence that, for each *odd* j, $a_j = -a_{-j}$, so that the formula

$$\frac{\sinh js\alpha}{\sinh s\alpha} = \sum_{r=1}^{j} \mathrm{e}^{(j-2r+1)\alpha s}$$

may be used to simplify (2.8) into

$$A(s) = \Xi(s) \sum_{k=0}^{N} a_{2k+1} \left\{ 1 + 2 \sum_{j=1}^{k} \cosh 2j\alpha s \right\}, \tag{3.1}$$

whilst writing

$$a_{2k-1} = \frac{c_{2k-1}}{\sin\,\alpha(k+N) \sin\alpha(k-1-N)}, \tag{3.2}$$

simplifies (2.9) into

$$c_{2k-1} \tan\alpha(k-N) = c_{2k+1} \tan\alpha(k+N). \tag{3.3}$$

In this case, with the required *even* parity of A (s), $\Xi(s)$ is taken to be a constant Ξ_0. Other choices would lead to solutions not possessing the required boundedness properties of Ursell's edge waves (see EH1 for further details of K–L inversion). Note also, in (3.1) and elsewhere, that the inner sum is regarded as zero when $k = 0$.

When (3.1) is rewritten in the form

$$A(s) = \Xi(s) d_1 \left\{ 1 + 2 \sum_{k=1}^{N} \frac{d_{2k+1}}{d_1} \cosh 2ks\alpha \right\}$$

(see the Appendix) this may be substituted in (2.7) and the K–L inversion carried out termwise. This gives (with $\Xi = \Xi_0 \Rightarrow \lambda = 0$)

$$\phi(R,\theta) = \frac{\pi \Xi_0 d_1}{2} \left\{ \mathrm{e}^{-\kappa R \cos(\theta+\alpha)} + \sum_{k=1}^{N} \frac{d_{2k+1}}{d_1} \left(\mathrm{e}^{-\kappa R \cos(\theta+(2k+1)\alpha)} + \mathrm{e}^{-\kappa R \cos(\theta+(1-2k)\alpha)} \right) \right\}$$

which, in view of (2.10) and the result in the Appendix, is identical to the expression written (but not systematically derived) by Ursell (1952).

4. Roseau's alternative edge waves

For the case $J = 2N,\ N \in Z$ solutions are found which do not possess the boundedness property at $R = 0$. These were first written by Roseau (1958) in a comprehensive study which discussed in great detail a wide class of solutions to the problem delineated by the system (2.1)–(2.5). Of that class, interest here is limited to those solutions consistent with (2.6) and, in view of Roseau's observations that the

https://doi.org/10.1017/S0022112098003899 Published online by Cambridge University Press

waves similarly decayed exponentially as $x \to \infty$, these will be denoted 'alternative edge waves' or 'edge waves of the second kind'.

The concern is now with a_j, j even. To this end, note from (2.9) that, for *even* j, $a_j = a_{-j}$ and, moreover, following an inductive argument similar to the one used for odd j in the Appendix, that

$$a_0 + 2\sum_{k=1}^{N} a_{2k} = 0. \tag{4.1}$$

Thus it follows from (2.8) that

$$A(s) = \frac{\Xi(s)}{\sinh s\alpha}\left\{a_0 + 2\sum_{j=1}^{N} a_{2j}\cosh 2js\alpha\right\}, \tag{4.2}$$

where, in view of (4.1), the term in the brace will have a double zero at $s = 0$. It will now be necessary to adopt *odd* parity for the i-periodic function Ξ and the choice

$$\Xi(s) = \coth \pi s \tag{4.3}$$

satisfies the required conditions: (i) it does not violate asymptotics as $s \to \infty$; (ii) it introduces no new singularities in the strip $0 < \mathrm{Im}(s) < 1$; (iii) it will render $A(s)$ with a simple pole at $s = -\mathrm{i}$ and a finite limit as $s \to 0$. These requirements were shown rigorously in EH1 to be those required for the proof of solution. Moreover, (4.1) enables the elimination of the divisor in (4.2) which therefore becomes

$$\begin{aligned} A(s) &= 2\Xi(s)\sum_{j=1}^{N} a_{2j}\frac{\sinh^2 js\alpha}{\sinh s\alpha} = 2\Xi(s)\sum_{j=1}^{N} a_{2j}\sinh js\alpha\sum_{r=1}^{j}\mathrm{e}^{(j-2r+1)\alpha s} \\ &= 2\Xi(s)\sum_{j=1}^{N} a_{2j}\sum_{r=1}^{j}\sinh(2r-1)s\alpha = 2\Xi(s)\sum_{r=1}^{N} d_{2r}\sinh(2r-1)s\alpha, \end{aligned}$$

where, consistent with the notation in the Appendix,

$$d_{2k} = \sum_{j=k}^{N} a_{2k}.$$

The potential of the 'second kind' edge waves is therefore given by

$$\phi(R,\theta) = \lambda K_0(\kappa R) + 2d_2\sum_{m=1}^{N} B_{m,N}\int_0^{\infty}\coth \pi s\sinh(2m-1)s\alpha \times\cosh s(\theta+\alpha)\,K_{is}(\kappa R)\,\mathrm{d}s, \tag{4.4}$$

where, to be consistent with Ursell's type of notation,

$$B_{m,N} = (-)^{m-1}\prod_{r=1}^{m-1}\frac{\tan\alpha(N-r)}{\tan\alpha(N+r)}; \quad B_{1,N} = 1, \tag{4.5}$$

from the final results in the Appendix. Note that (2.10) is now equivalent to the dimensional frequency relation

$$\sigma^2 = gk\,\sin 2N\alpha \tag{4.6}$$

thus giving a discrete spectrum of wavenumbers interlacing those of Ursell's edge

https://doi.org/10.1017/S0022112098003899 Published online by Cambridge University Press

waves which were given by

$$\sigma^2 = gk \sin(2N+1)\alpha. \tag{4.7}$$

In (4.4) λ is given by

$$\lambda = -\mathrm{i}\pi\kappa \sin\alpha \operatorname{Res}_{s=-\mathrm{i}} \left\{ d_2 \sum_{m=1}^{N} B_{m,N} \coth \pi s \sinh(2m-1)s\alpha \right\}$$

$$= -\kappa d_2 \sin\alpha \sum_{m=1}^{N} B_{m,N} \sin(2m-1)\alpha. \tag{4.8}$$

There are two fundamental ways of facilitating computation of (4.4). One is to determine the (exponential) far-field asymptotics of the K–L inversion leaving only a 'remainder' term to be computed. The other is to construct a uniformly convergent near-field expansion by conventional use of the residue theorem. Both methods were fully discussed and proved in EH1 and only the results will be given here. The near-field expansion is considered first. It is convenient to set the arbitrary constant $d_2 = 1$.

With the abbreviation $\vartheta_m = (2m-1)\alpha$, this expansion may be written

$$\phi = \log\left(\frac{\kappa R}{2}\right) \sum_{\rho=0}^{\infty} A_\rho \left(\frac{\kappa R}{2}\right)^\rho - \sum_{\rho=0}^{\infty} C_\rho \left(\frac{\kappa R}{2}\right)^\rho, \tag{4.9}$$

where

$$A_\rho = \sum_{m=1}^{N} B_{m,N} \sum_{j=0}^{[\rho/2]} \frac{1}{j!} \frac{e_{m,\rho-2j}}{(\rho-j)!},$$

$$C_\rho = \sum_{m=1}^{N} B_{m,N} \sum_{j=0}^{[\rho/2]} \frac{1}{j!} \frac{\{e_{m,\rho-2j}\,\psi(\rho-j+1) - (-)^\rho \mu_{\rho-2j} \Theta_m(\rho-2j)\}}{(\rho-j)!}$$

having set $e_{m,0} = \kappa \sin\alpha \sin\vartheta_m$; $e_{m,k} = (-)^k \mu_k \sin k\vartheta_m \cos k(\theta+\alpha)$, $k > 0$. In the above, ψ is the usual digamma function and $\mu_k = 1$ if $k = 0$, $\mu_k = 2$ otherwise. Additionally,

$$\Theta_m(k) = \vartheta_m \cos k\vartheta_m \cos k(\theta+\alpha) - (\theta+\alpha)\sin k\vartheta_m \sin k(\theta+\alpha)$$

for convenience.

To understand the limitations of (4.9) it is only necessary to consider the analogy with the Ursell waves, where a similar procedure would yield an expansion which is equivalent to writing the Maclaurin series of each exponential function of the Ursell modes and changing orders of summation. This series will be uniformly convergent but will require an inordinately large number of terms for computational accuracy when κR is large. In the continuous spectrum case, the author has noted (EH1) that six-digit accuracy in the solution could be maintained with 72 terms of the series as far as $R = 15$. Here however, the larger values of κ more severely limit its use and for shallower beaches (say $\alpha < \pi/10$) it is impractical to use the formula beyond $R = 10$. 'Desk-top' computations (avoiding full numerical quadrature of (4.4) with the help of a NAG routine and methods discussed by Ehrenmark 1995) therefore require a combination of the near- and far-field expansions.

https://doi.org/10.1017/S0022112098003899 Published online by Cambridge University Press

For the far-field expansion, it follows, after rearranging (4.4) and inverting suitably, that

$$\phi = \lambda K_0(\kappa R) + \frac{\pi}{2}\sum_{m=1}^{N} B_{m,N}\{\mathrm{e}^{-\kappa R\cos(2(m-1)\alpha-\theta)} + \mathrm{e}^{-\kappa R\cos(2m\alpha+\theta)}\}$$
$$+ 2\sum_{m=1}^{N} B_{m,N}\int_0^\infty \frac{\sinh[(2m-1)\alpha-\pi]s}{\sinh \pi s}\cosh s(\theta+\alpha)\,K_{is}(\kappa R)\,\mathrm{d}s. \quad (4.10)$$

The integrand in the 'remainder term' converges at least like $\exp(-\pi s/2)$ and the inversion is carried out numerically without any difficulty (see Ehrenmark 1995). Moreover, it was established as a theorem in EH1 that if $f(s) \in L(0,\infty)$, and if for some s_0, $|f(s)| < \exp(-\lambda s)$ for some $\lambda > 0, \forall s > s_0$ then

$$F(x) \equiv \int_0^\infty f(s)K_{is}(x)\,\mathrm{d}s \sim \mathrm{e}^{-x}\left(\frac{\pi}{2x}\right)^{1/2}\int_0^\infty f(s)\mathrm{d}s. \quad (4.11)$$

This estimate may be used for $\kappa R >> 1$ in the last term of (4.10) for $m = 2, 3, \ldots, N$. If $m = 1$ a similar result holds if, for some $\delta > 0$, $\theta \leqslant -\delta$. If $\theta = 0$, it follows that

$$\int_0^\infty \frac{\sinh(\alpha-\pi)s}{\sinh \pi s}\cosh s\alpha\,K_{is}(\kappa R)\,\mathrm{d}s = -\frac{\pi}{2}\mathrm{e}^{-\kappa R} + O\left(\mathrm{e}^{-\kappa R}\left(\frac{1}{\kappa R}\right)^{1/2}\right).$$

This facilitates an asymptotic expansion on the surface $\theta = 0$,

$$2\phi/\pi \sim -B_{1,N}\mathrm{e}^{-\kappa R} + \sum_{j=1}^{N-1}(B_{j,N} + B_{j+1,N})\mathrm{e}^{-\kappa R\cos 2j\alpha} + B_{N,N}\mathrm{e}^{-\kappa R\cos 2N\alpha}. \quad (4.12)$$

Note in particular from the above that, for waves at the cut-off frequency, whence $N = \pi/2\alpha$, the exponential decay as $x \to \infty$ is lost, as it is also for the uniformly bounded edge waves of Ursell. Evans & Kuznetsov (1997, p. 130) define 'trapped' waves as those for which a certain energy measure, namely

$$I \equiv \int_\Omega |\nabla\Phi|^2\mathrm{d}V + \int_{\partial\Omega\cap F}\{\Phi^2\}\,\mathrm{d}S < \infty, \quad (4.13)$$

is satisfied (here Ω is the body of fluid and F is the free surface). Clearly (4.13) will be violated by the cut-off modes. Bearing in mind then the formulation of the oblique incidence problem in the continuous spectrum (Peters 1952; Whitham 1979; EH1) it seems reasonable to regard the cut-off modes as part of that spectrum thus representing waves which are incident at 90° and that therefore their profile, which for 0° incidence is asymptotically uniform in the longshore direction, is now instead asymptotically uniform in the cross-shore direction (Ursell 1952).

Moreover, the identification of the continuous spectrum solutions by $I = \infty$ is not always helpful. It fails to distinguish the logarithmically singular solutions from the ones that are bounded there, the latter set of standing waves being attributed a property of completeness by Minzoni & Whitham (1977), which is evidently not satisfied by the former group. Furthermore, other classes of unbounded solutions discussed first by Lehman (1954) and then (for three-dimensional motion) by Roseau (1958) are known to exist which, it would seem, would not normally be observable on minimum energy norm arguments.

https://doi.org/10.1017/S0022112098003899 Published online by Cambridge University Press

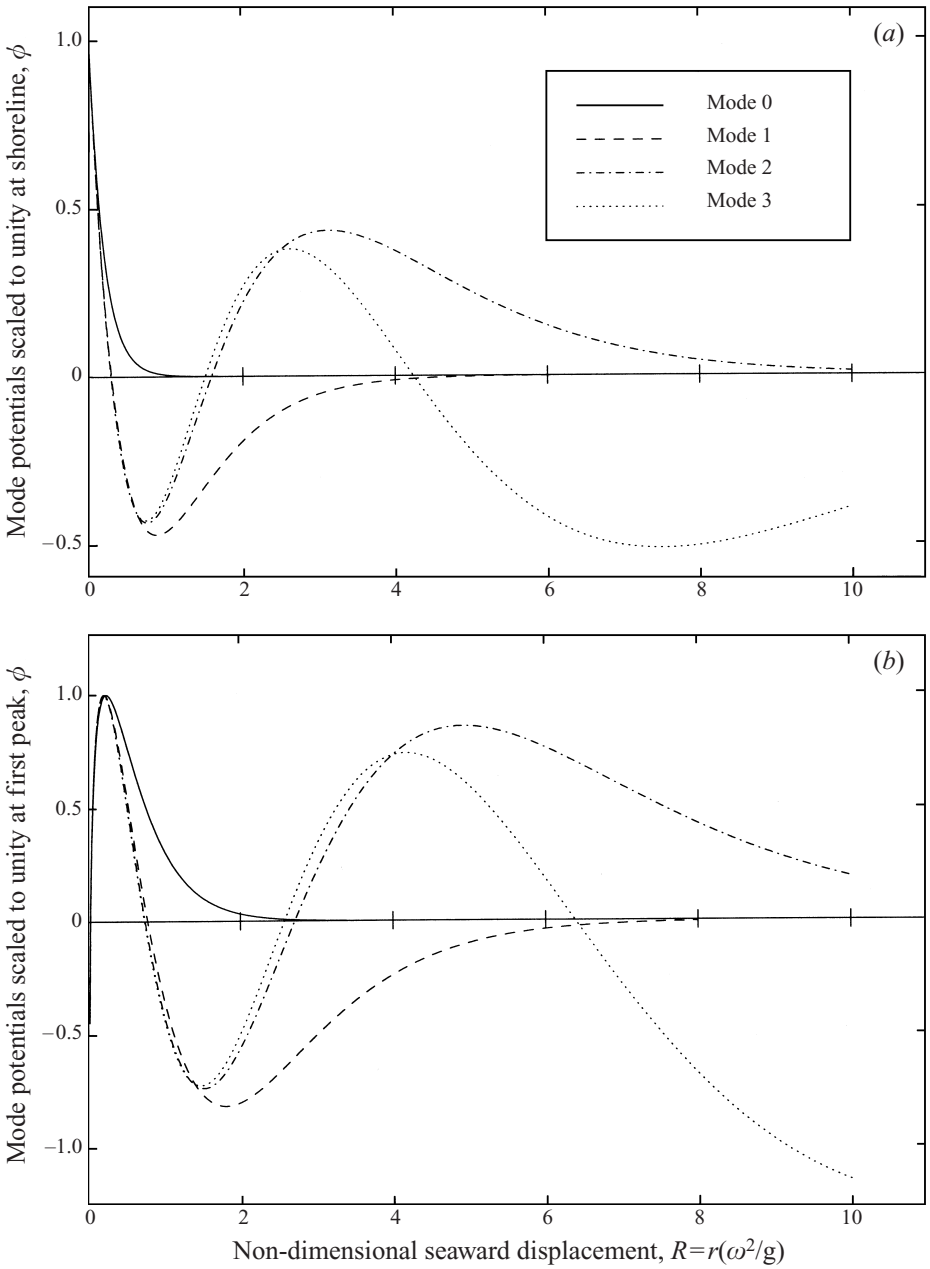


FIGURE 1. (*a*) Ursell and (*b*) Roseau edge wave surface profiles on $\alpha = \pi/17$, modes $N = 0, 3$.

5. Computation of profiles and streamlines

Figure 1(*a*) shows free surface profiles for the first four modes of the bounded Ursell waves (denoted E1) whilst figure 1(*b*) displays a similar range of modes for the second-kind edge waves (denoted E2). The calculations are performed with a beach angle $\alpha = \pi/(2q+1)$ (in this case) for $q = 8$. This prevents the occurrence of cut-off modes. The inner expansion (4.9) has been combined suitably with the asymptotic expression (4.12) to compute E2. As a check on the accuracy of computations, a useful device

https://doi.org/10.1017/S0022112098003899 Published online by Cambridge University Press

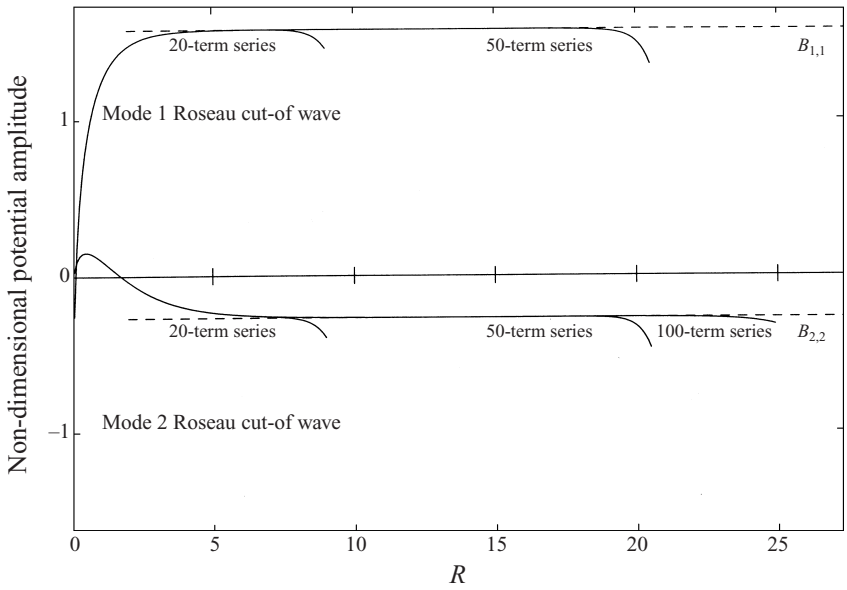


FIGURE 2. Cut-off amplitudes computed from (4.9) – note asymptotes $B_{N,N}$.

is to compute a cut-off mode. For this mode, with $2N\alpha = \pi/2$, it follows from the asymptotic relation (4.6) that $\phi \sim B_{N,N}\pi/2$. This makes it very easy to see from the numerical output the limit of acceptability of the inner expansion for increasing values of R and therefore indicates when the number of terms of the expansion has to be increased or the far-field approximation (4.12) invoked. Results of this are displayed in figure 2. Note also that each mode E1 is normalized with respect to the shoreline value whilst modes E2 are normalized with respect to their first peak values (the rationale for doing this will become evident).

Consider next the determination of dividing streamlines. These emanate from points on the bed and rise to the surface. Classical two-dimensional stagnation point theory suggests that the intersection with the bed is orthogonal whilst that with the surface, in general, will not be. If we write $k\boldsymbol{x} \equiv \boldsymbol{X}$ for convenience, then the X-coordinates of any stagnation points (here denoting points where stagnation occurs if the longshore motion is also zero) on the bed, in the case of Ursell's edge waves, are given by

$$\mathrm{e}^{-X\,\mathrm{scc}\alpha} + 2\sum_{m=1}^{N} A_{m,N}\cos 2m\alpha\,\mathrm{e}^{-X\,\cos\,2m\alpha\mathrm{scc}\alpha} = 0 \tag{5.1}$$

where the $A_{m,N}$ are Ursell's coefficients (defined herein in the Appendix).

The simplest case $N = 1$, $\alpha \leqslant \pi/6$, leads to a single bed stagnation point at

$$x = \frac{\cos\,\alpha}{2k\sin^2\alpha}\,\ln\left(\frac{\tan 2\alpha}{2\tan\alpha\,\cos\,2\alpha}\right)$$

and for the 'cut-off' mode when $\alpha = \pi/6$, $\kappa R = 2\ln 3$. The 'trajectory' of this point as the bed slope angle is decreased is shown in figure 3. For the case $N = 2$, $\alpha \leqslant \pi/10$, two stagnation points, which are readily determined numerically, are found on the bed. The trajectories of these as α decreases are also shown in figure 3 together with similar trajectories for the stagnation points of the first two Roseau modes. Clearly the number of stagnation points (and therefore also dividing streamlines) is equal to N.

https://doi.org/10.1017/S0022112098003899 Published online by Cambridge University Press

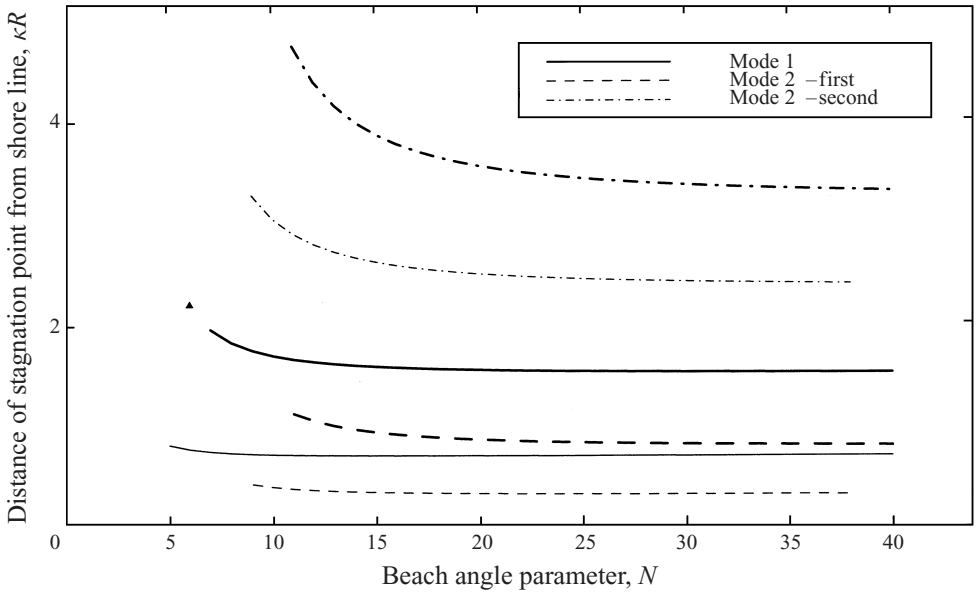


FIGURE 3. Bed Stagnation-point migration with beach slope. Thin lines: Roseau waves, $\kappa = 1/\sin((2M+1)\alpha)$; thick lines: Ursell waves, $\kappa = 1/\sin(2M\alpha)$. Physical displacement $r = Rg/\omega^2$. Solid triangle shows the exact mode 1 Ursell cut-off value.

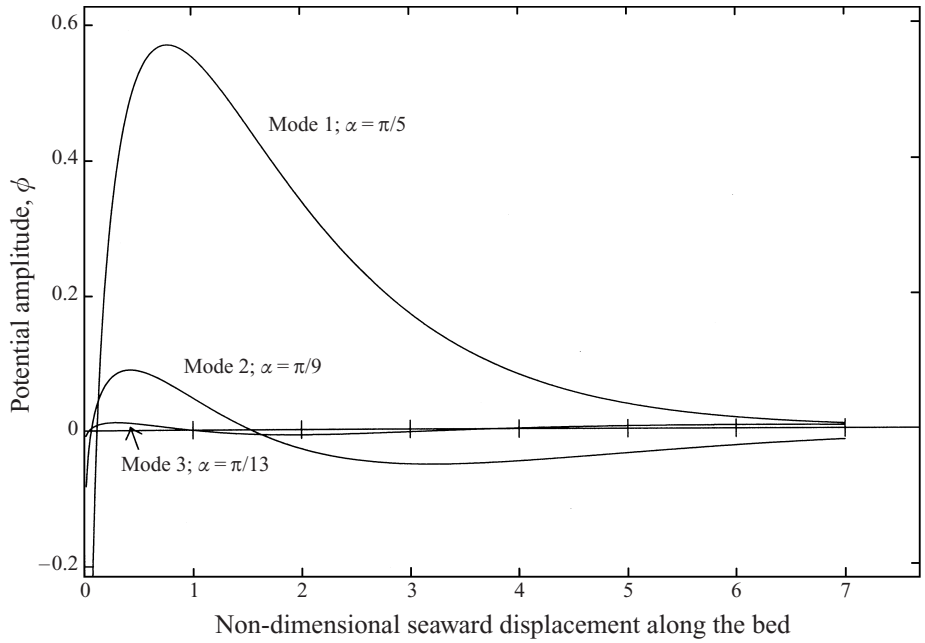


FIGURE 4. Sea-floor potential: Roseau modes 1, 2, 3; $\alpha = \pi/(q+1)$.

Note that the physical position will depend on wave frequency so that, for example, a laboratory E2 Mode 1 wave (E2,1) of typical frequency 1.5 Hz will have its stagnation point at about 9.5 cm from the shore line on a 30° inclination. In the field (see §6 below) the same mode operating at, say 0.02 Hz on an inclination $\tan^{-1} 0.025$ would

https://doi.org/10.1017/S0022112098003899 Published online by Cambridge University Press

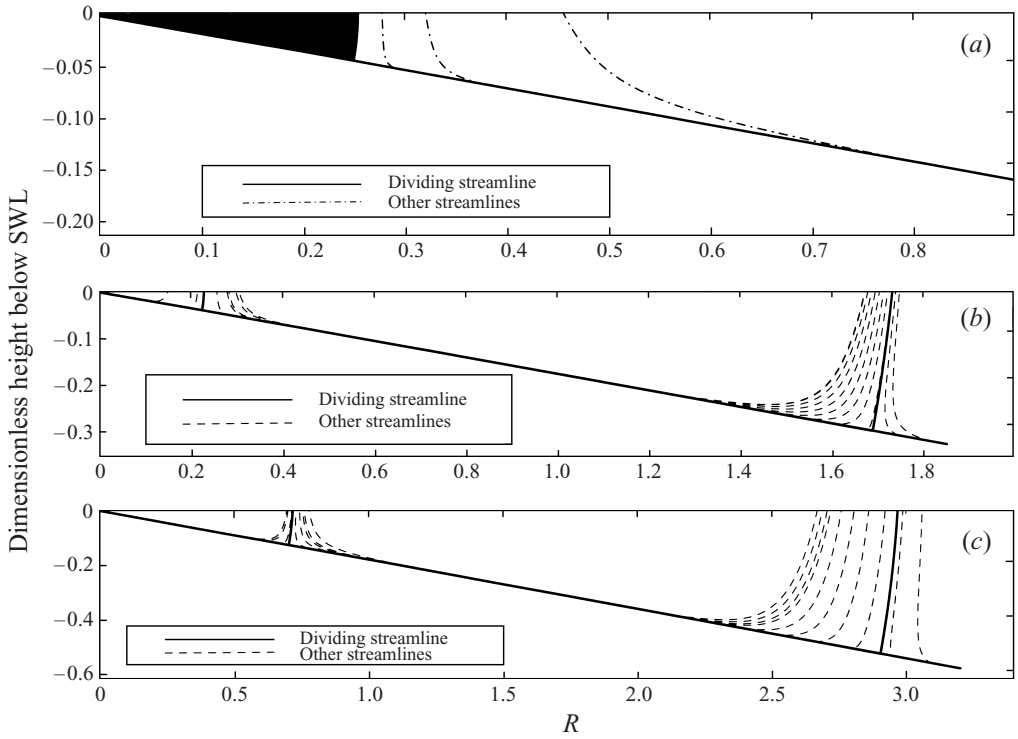


FIGURE 5. Dividing lines and other streamlines computed by fourth-order Runge–Kutta integration: (*a*) Roseau wave mode 1; (*b*) Roseau wave mode 2; (*c*) Ursell wave mode 2 ($\alpha = \pi/17$).

exhibit this point at about 21 m from shore, whilst on an inclination $\tan^{-1} 0.046$ the same feature would be observed at about 40 m.

Figure 4 shows potential distributions on the bed for three E2 cases near cut-off values. Again, it can be seen that stagnation points exist on the bed, here indicated by the extrema of the curves shown.

Figure 5(*a*) shows the computation of the E2,1 dividing streamline (D) for the case $\alpha = \pi/17$. This was obtained from a Runga–Kutta order-4 integration (RK4) commenced at a very small distance perpendicularly above the seafloor at the stagnation point. The method was first tested for numerical robustness by adopting the approach of Kuznetsov *et al.* (1998) whereby the streamline determined is 'retraced' by an RK4 application started at the first endpoint. Stream lines shoreward and seaward of D were also computed, the latter being displayed whilst the former are obscured by the 'shadow' of D to demonstrate that the wave E2,1 exists in a bounded state if this shadow region is made into a solid cylinder. The arc D is nearly circular; the (non-dimensional) radius shown in figure 5(*a*) varies monotonically from 0.253766 at the bed to 0.254209 at the free surface. Figures 5(*b*) and 5(*c*) display similar computations for the two dividing streamlines of respectively modes E2,2 and E1,2. Thus it can be seen that there is very little qualitative difference in behaviour between the Ursell and the Roseau waves if a small region surrounding the origin is removed from the flow. Again this can be done physically by making into a solid the shadow region behind either of the two dividing streamlines. In that case, the profile of the E2 modes is a maximum at the 'initial' point where D intersects the free surface and it is this similarity with the profile of classical E1 modes maxi-

https://doi.org/10.1017/S0022112098003899 Published online by Cambridge University Press

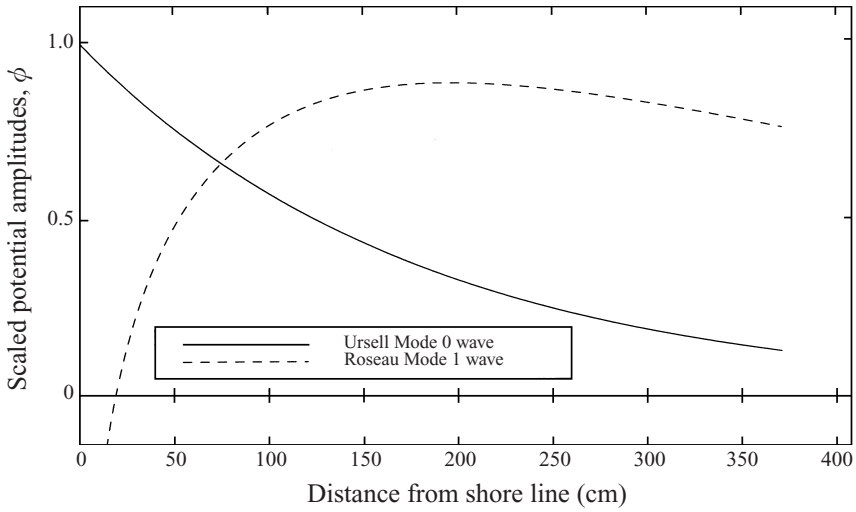


FIGURE 6. Ursell experiment I parameters: surface profiles; bed inclination $\alpha = 37.6°$.

mized at the shore line which prompted the normalization referred to earlier for E2 modes.

Moreover, with the E1 modes also existing in the presence of solid longshore near-circular cylinders, the number of which possible in a given situation equates to the mode number, one can argue that E1 and E2 modes are almost self-similar each type existing with cylinders of alternating radii or, with the scaling $R = r\omega^2/g$, that the cylinders are near similar but the frequencies alternate. In fact the numerical evidence is that, whilst the scaling of cylinders is quite similar, they are by no means identical although with the radius of the smallest cylinder approaching zero with decreasing bed slope (at fixed frequency), any discrepancies in shapes of solid cylinders determined by E1 and E2 will become undetectable – at least within the realms of linearized theory approximations.

6. Observations from past laboratory and field work

In order to examine, at least qualitatively, the relationship between the present theory and existing observational evidence, some of the results of four particular collections of experiments are considered: (i) the laboratory data of Ursell (1952); (ii) the laboratory data of Guza & Bowen (1976); (iii) the field results at Santa Barbara published by Oltman-Shay & Guza (1987); (iv) the field results at Torrey Pines published by Oltman-Shay & Guza (1987).

The laboratory tanks were generally shallow (23 cm (i) and 30 cm (ii)) but long enough (370 cm (i) and 200 cm (ii)) to eliminate significant cross-shore resonances. It is also stressed that long-shore wavenumbers (κ) were restricted by cross-shore boundaries. In (i) these were further complicated by a secondary arrangement of vertical walls also inducing a resonant frequency at the cut-off value measured in a wider communicating canal of uniform depth. The results of the paper are therefore not really applicable to the present simplistic model of an infinite plane beach; nevertheless the scarcity of data makes at least a cursory examination of the results tempting. Similarly the results of (ii) will be considered only fleetingly and attention instead concentrated on more careful examination of the field results (iii) and (iv).

https://doi.org/10.1017/S0022112098003899 Published online by Cambridge University Press

In each case (i–iv) there are specific measures of the beach slope $\alpha_{k,i}$ (which, of course, for (iii) and (iv) are only average values). Those in (i) are 37.6° and 29.5° and, for the range of frequencies considered, the first value supports (on an infinite plane beach) only mode 0 (Stokes' wave) of the Ursell modes, whilst the second value supports also a mode 1 wave. Both values support only the fundamental mode 1 Roseau wave (E2,1). In his discussion of experiment I, Ursell (1952) refers to the sensitivity of measurements in relation to the placement of the response measuring device. This is because of the standing nature of the cross-shore oscillations. The modes referred to are shown here in figure 6 although of course the relative amplitudes are indeterminate. Figure 2 of Ursell (1952) shows observation of the mode 0 Stokes edge wave (123 c min^{-1}) beyond question. The second peak shown is attributed to a resonance with the cut-off mode in the lower end of the canal, expected at 157 c min^{-1} but actually appearing at about 163 c min^{-1}. The positioning of the optical plane reading the response is deemed to be critical and it is remarked how (in a third experiment) abnormally low amplitudes at 140 c min^{-1} are attributed to a repositioning.

Interest here would be in assessing if there is any evidence of the E2,1 wave present in the data exhibited by Ursell. By (4.6) this wave would be oscillating at the frequency $\omega/2\pi = (g \sin 75.2^\circ/4\pi b_1)^{1/2} \approx 155$ c min^{-1}. (Here b_1=11.4 cm denotes the width of the canal.) The frequency value is therefore so close to the cut-off mode (157 c min^{-1}) as to make any proper assessment impossible. It might conceivably be argued that, if there is 'contamination of the data' by the R1 wave then this could be partly responsible for the widening of the peak bandwith to the left of the experimental peak. This asymmetry was attributed by Ursell purely to the positioning of measuring equipment which was evidently extremely close to the beach line (presumably only centimetres away) to capture optically the maximum slope of the Stokes edge wave. It would therefore also (see figure 6*a*) not be in a region of maximum influence of an E2,1 wave, as always on the assumption that viscosity would attenuate the (logarithmically) large values occurring within a few centimetres of the shoreline.

Guza & Bowen (1976), investigating nonlinear interaction amongst edge waves, also report laboratory results which could have been of interest. Unfortunately, here again, the tank dimensions chosen were such as to make the frequency ($\approx$ 1.72 Hz) of the observed second resonance, denoted (2, 0) in their notation, very close to the theoretical frequency ($\approx$ 1.68 Hz) of an E2, 1 wave under the same tank parameters.

Two significant field studies have been examined in the context of edge waves by Oltman-Shay & Guza (1987). At the Santa Barbara site the beach slope varies considerably between a steep 'centre section' of 0.06 with less-steep sections seaward (0.01) and shoreward (0.045). The second site, at Torrey Pines, San Diego, was reported to have a more uniform beach slope, approximately 0.025. The sensor arrays were arranged in the surf zone and parallel to the foreshore respectively at about 26 m and 66 m from the mean shore line. In order to graph qualitatively the theoretically predicted edge wave modes, the Santa Barbara beach is assumed to have a gradient 0.046 (ridge value given by authors). The number of Ursell modes supported on a plane beach of this gradient is 17 whilst the number for the Torrey Pines beach slope is 31. The two primary-mode Ursell and Roseau relative wave height response curves for the two simulations are shown in figures 7(*a*) and 7(*b*) respectively.

The identification, in the previous section, of the dividing streamline D for the E2,1 wave allows us to speculate that (in view of the exponentially decaying profile beyond D) the maximum impact on longshore motion of any 'E2 contamination'

https://doi.org/10.1017/S0022112098003899 Published online by Cambridge University Press

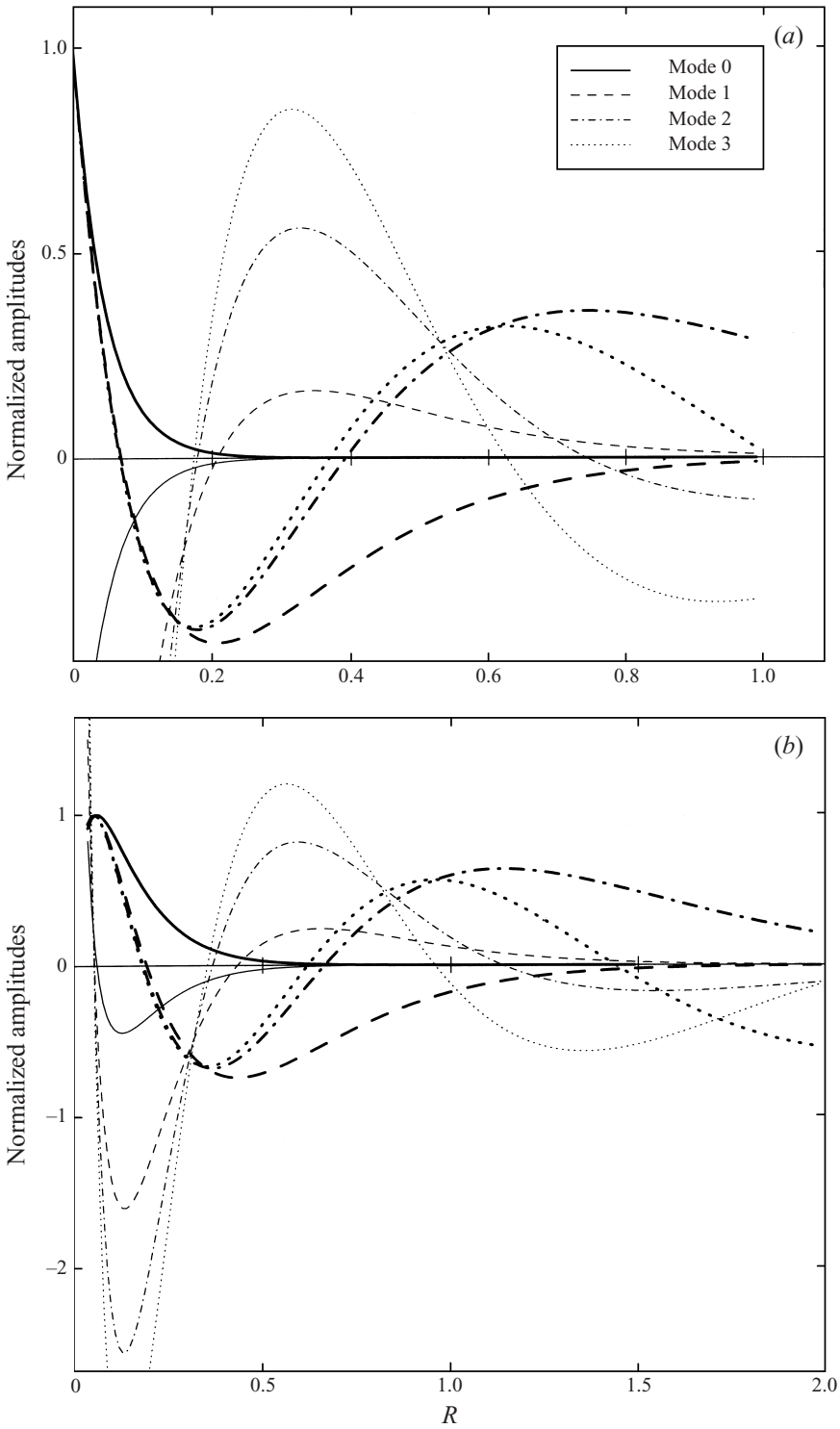


FIGURE 7. Santa Barbara parameters: horizontal surface velocities, (*a*) Ursell wave modes, (*b*) Roseau wave modes. Thin lines: cross-shore flow; thick lines: long-shore flow. Note that the true displacement $r = Rg/\omega^2$, where $\omega/2\pi$ =frequency.

https://doi.org/10.1017/S0022112098003899 Published online by Cambridge University Press

would be close to the location of D. The impact on cross-shore motion will however be maximized further seaward (see figure 6*b*). This follows because the behaviour of E2 waves beyond D is similar to E1 waves if one were to regard D as an 'imaginary origin' for E2 waves. Perhaps the most striking observation of energetics observed between Ursell modes 0 and 1 (thus appropriate to Roseau mode 1) is found in figure 13 of Oltman-Shay & Guza (1987) which reports occurrence of this at between 0.03 and 0.04 Hz for the longshore current on the Santa Barbara beach. With the wave sensors at 26 m and the slope 0.046, the equivalent range of κR is $1.10 \leqslant \kappa R \leqslant 1.97$. The asymptotic location of D for all small slope angles is just less than 0.7. The sensors are therefore just within range of a significant E2 signal (see figure 6*c*) at least at the lower end of the frequency range as also noted by Oltman-Shay & Guza (1987) (figure 12) to reveal the frequency dependence of response (at fixed locations) of the first three Ursell modes.

7. Summary

The presentation of a new method to solve the classical linearized beach problem over the discrete spectrum has enabled the construction of a simple computational framework from which the unbounded edge wave solutions of Roseau (1958) can be studied in detail. In particular a near-field expansion has proved to be of great value to the desk-top user and all computations of these waves presented in this work were evaluated in this way.

One of the main results of the paper is the demonstration that a (two-dimensional cross-shore) dividing field line exists, for all modes of the Roseau waves. This permits the waves to exist in a uniformly bounded state in the presence of a solid cylinder, placed at the shoreline, whose generators coincide with the shadow region of the dividing streamline. Moreover, for the Nth mode, N such streamlines exist giving a variety of possible cylindrical 'exterior wave guides' to support the propagation of new beach edge waves. As the profile of the cylinders is almost circular they provide an effect akin to that of an overhanging cliff. Similar situations can be constructed for the Ursell waves (and – although probably with less physical interest – for the classical continuous spectrum two-dimensional standing wave solutions). The radii of the cylinders depend on beach gradient and on the frequency of the waves propagated but, for laboratory waves of $O(1)$ Hz the radius of the smallest cylinder is only a few centimetres on a gradient of about 1:3. This should make practical a laboratory test in a large three-dimensional wave facility to evaluate whether or not the new waves can actually be observed. Study of some available evidence from both the field and the laboratory has failed to yield any significant conclusions.

Finally, it is argued that, with infinite plane beaches unlikely in practice and with the radius of the solid cylinder required to support bounded Roseau wave modes becoming very small as beach slope approaches zero, the likelihood is that a plane beach with such a solid cylinder is not necessarily less representative in linear theory than the infinite plane beach. It is therefore suggested that Roseau modes could be observed in the field but that the cross-shore observation points have to be chosen carefully.

The author is indebted to the Leverhulme Trust for funding under grant No. F/405/B.

https://doi.org/10.1017/S0022112098003899 Published online by Cambridge University Press

Appendix.

For the case $J = 2N + 1$, the recurrence relation (2.9) may be rewritten

$$a_{2k-1} \cos \alpha(k+N) \sin \alpha(k-N-1) = a_{2k+1} \cos \alpha(k-N) \sin \alpha(k+N+1)$$

from which can be written the general solution

$$\frac{a_{2m+1}}{a_1} = -\frac{\sin \alpha N \sin \alpha(N+1)}{\sin \alpha(m+N+1) \sin \alpha(m-N)} \prod_{r=1}^{m} \frac{\tan \alpha(r-N)}{\tan \alpha(r+N)}.$$

The double summation in (3.1) is now expressed in the form

$$A(s) = \Xi(s) \left\{ d_1 + 2 \sum_{k=1}^{N} d_{2k+1} \cosh 2ks\alpha \right\}$$

so that,

$$d_{2N+1} = a_{2N+1},\ d_{2N-1} = d_{2N+1} + a_{2N-1},\ \ldots,\ d_{2(N-j)+1} = d_{2(N-j)+3} + a_{2(N-j)+1}, \ldots.$$

Now note that

$$d_{2N-1} = a_{2N+1} \left(1 + \frac{\sin \alpha(2N+1)}{\cos 2\alpha N \sin \alpha} \right) = -a_{2N+1} \frac{\tan 2N\alpha}{\tan \alpha}$$

and that, similarly,

$$d_{2N-3} = a_{2N+1} \frac{\tan 2N\alpha \tan(2N-1)\alpha}{\tan \alpha \tan 2\alpha}.$$

It will be established, by induction, that

$$d_{2(N-j)+1} = (-)^j a_{2N+1} \frac{\tan 2N\alpha \tan(2N-1)\alpha \ldots \tan(2N-j+1)\alpha}{\tan \alpha \tan 2\alpha \ldots \tan j\alpha}.$$

The hypothesis is true for $j = 1$, $j = 2$. Assume that it is true for $j - 1$. Then

$$\begin{aligned} d_{2(N-j)+1} &= d_{2(N-j)+3} + a_{2(N-j)+1} \\ &= (-)^{j-1} a_{2N+1} \frac{\tan 2N\alpha \ldots \tan(2N-j+2)\alpha}{\tan \alpha \ \ldots \tan(j-1)\alpha} + a_{2(N-j)+1} \\ &= (-)^{j-1} a_{2N+1} \frac{\tan 2N\alpha \ldots \tan(2N-j+2)\alpha}{\tan \alpha \ \ldots \tan(j-1)\alpha} \\ &\quad \times \left\{ 1 - \frac{\sin(2N+1)\alpha}{\cos(2N+1-j)\alpha \sin j\alpha} \right\} \\ &= (-)^j a_{2N+1} \frac{\tan 2N\alpha \ldots \tan(2N-j+1)\alpha}{\tan \alpha \ldots \tan j\alpha}. \end{aligned}$$

Finally, write

$$\frac{d_{2m+1}}{d_1} = (-)^m \frac{\prod_{r=1}^{m} \tan(N-m+r)\alpha}{\prod_{r=1}^{m} \tan(N+r)\alpha}$$

so that the coefficients $A_{m,n}$ defined by Ursell (1952) are recovered here by

$$A_{m,N} = \frac{d_{2m+1}}{d_1}.$$

https://doi.org/10.1017/S0022112098003899 Published online by Cambridge University Press

In the case where instead $J = 2N$, similarly

$$\frac{a_{2m}}{a_0} = \frac{-\cos\,\alpha N \sin\alpha N}{\cos\,\alpha(m+N)\;\sin\,\alpha(m-N)} \prod_{r=1}^{m} \frac{\tan\alpha(r-N)}{\tan\,\alpha(r+N)}$$

and

$$\frac{d_{2m}}{d_2} = (-)^{m-1} \prod_{r=1}^{m-1} \frac{\tan\alpha(N-r)}{\tan\,\alpha(N+r)};\; m = 2,3,4\ldots .$$

REFERENCES

Blondeaux, P. & Vittori, G. 1995 The nonlinear excitation of synchronous edge waves by a monochromatic wave normally approaching a plane beach. *J. Fluid Mech.* **301**, 251–268.

Body, G. & Ehrenmark, U. T. 1999 Second harmonics generated by a bounded standing wave on a plane beach of arbitrary slope. *Q. J. Mech. Appl. Maths* (in press).

Booij, N. 1983 A note on the accuracy of the mild-slope approximation. *Coastal Engng* **7**, 191–203.

Bruce, J. 1998 PhD Dissertation, London Guildhall University (in preparation).

Ehrenmark, U. T. 1995 The numerical inversion of two classes of Kontorovich–Lebedev transform by direct quadrature. *J. Comput. Appl. Maths* **61**, 43–72.

Ehrenmark, U. T. 1996 Eulerian mean current and Stokes drift under non-breaking waves on a perfect fluid over a plane beach. *Fluid Dyn. Res.* **18**, 117–150.

Ehrenmark, U. T. 1998 Oblique wave incidence on a plane beach: The classical problem revisited. *J. Fluid Mech.* **368**, 291–319 (referred to herein as EH1).

Evans, D. V. 1988 Mechanisms for the generation of edge waves over a sloping beach. *J. Fluid Mech.* **186**, 379–391.

Evans, D. V. 1989 Edge waves over a sloping beach. *Q. J. Mech. Appl. Maths* **42**, 131–142.

Evans, D. V. & Kuznetsov, N. 1997 Trapped modes. In *Gravity Waves in Water of Finite Depth* ed. J. N. Hunt), Chap. 4. Computational Mechanics Publications, Southampton UK 1997.

Guza, R. T. & Bowen, A. J. 1976 Finite amplitude edge waves. *J. Mar. Res.* **34**, 269–293.

Kuznetsov, N., Porter, R., Evans D. V. & Simon, M. J. 1998 Uniqueness and trapped modes for surface-piercing cylinders in oblique waves. *J. Fluid Mech.* **365**, 351–368.

Lehman, R. S. 1954 Developments in the Neighborhood of the beach of surface waves over an inclined bottom. *Commun. Pure Appl. Maths* **7**, 393–439.

Miles, J. W. 1990*a* Parametrically excited standing edge waves. *J. Fluid Mech.* **214**, 43–57.

Miles, J. W. 1990*b* Wave reflection from a gently sloping beach. *J. Fluid Mech.* **214**, 59–66.

Minzoni, A. A. 1976 Non-linear edge waves and shallow water theory. *J. Fluid Mech.* **74**, 369–374.

Minzoni, A. A. & Whitham, G. 1977 On the excitation of edge waves on beaches. *J. Fluid Mech.* **79**, 2, 273–287.

Oltman-Shay, J. & Guza, R. T. 1987 Infragravity edge wave observations on two california beaches. *J. Phys. Oceanogr.* **17**, 644–663.

Peters, A. S. 1952 Water waves over sloping beaches and the solution of a mixed boundary value problem for $\Delta\varphi - k^2\varphi = 0$ in a sector. *Commun. Pure Appl. Maths* **5**, 87–108.

Roseau, M. 1951 Sur les mouvements ondulatoires de la mer sur une plage. *C. R. Acad. Sci. Paris* **232**, 479–481.

Roseau, M. 1952 Contribution à la théorie des ondes liguides de gravité en profondeur variable. *Publications Scientifiques et Techniques du Ministère de l'Air, Paris* 275.

Roseau, M. 1958 Short waves parallel to the shore over a sloping beach. *Commun. Pure Appl. Maths* **9**, 443–493.

Ursell, F. 1952 Edge waves on a sloping beach. *Proc. R. Soc. Lond.* A **214**, 79–97.

Watson, G. N. 1944 *A Treatise on The Theory of Bessel Functions.* Cambridge University Press.

Whitham, G. B. 1976 Nonlinear effects in edge waves. *J. Fluid Mech.* **74**, 353–368.

Whitham, G. B. 1979 *Lectures on Wave Propagation.* Tata Institute of Fundamental Research. Springer.

https://doi.org/10.1017/S0022112098003899 Published online by Cambridge University Press